

A 50 kW Liquid-Lithium Target for BNCT and Material-Science Applications

Michael Paul^{1,*}, Ido Silverman^{2,*}, Shlomi Halfon², Semion Sukoriansky³, Boris Mikhailovich³, Tala Palchan¹, Arkady Kapusta³, Arthur Shoihet⁴, Daniel Kijel², Alexander Arenshtam^{2,†} and Eli Barami^{2,3}

¹Racah Institute of Physics, Hebrew University, Jerusalem, Israel 91904

²Soreq Nuclear Research Center, Yavne, Israel 81800

³Department of Mechanical Engineering, Ben-Gurion University of the Negev, Beer-Sheva, Israel

⁴NRCN, Beer-Sheva, Israel

Abstract. A compact Liquid Lithium Target (LiLiT) has been operating at SARAF for several years with beam power of several kW (1.9-2.5 MeV, up to 2 mA). When bombarding the lithium with low energy protons neutrons are generated. The neutron source, mainly used for nuclear astrophysics research, was decommissioned in 2016 towards an upgraded model - with possible applications to Boron Neutron Capture Therapy (BNCT) and material-science studies. The improved version has been designed to sustain 50 kW proton beam power (2.5 MeV, ~20 mA) to provide sufficient neutron flux required for clinical BNCT application. The new model has a 50 mm wide lithium jet to enable dissipation of the higher beam power and an improved heat exchanger to remove the power to a secondary cooling loop. A new Annular Linear INduction electro-magnetic pump (ALIN) has been designed and built to provide the required lithium flow rate. Other mechanical improvements facilitate the maintenance of the system and the robustness of operation. Radiological risks due to the ${}^7\text{Be}$ produced in the reaction are reduced by using an integrated lead shielding of the lithium reservoir. An integrated neutron moderator is being designed to adjust the neutron energy to the spectrum best suited to BNCT. A low power (6 kW) model of the new design with a narrower nozzle (18 mm wide) and a rotating-magnet electro-magnetic pump is operating at SARAF to support the ongoing astrophysics and nuclear research program [1], [2]. To fulfill clinical BNCT, the upgraded LiLiT model will require an accelerator of appropriate energy and intensity. The design features of the new system are presented in this paper.

1 Background

Neutrons, penetrating non-ionizing particles, can be utilized in a form of radiotherapy generally termed today Neutron Capture Therapy (NCT). NCT was first suggested by G. L. Locher [3] as early as 1936, a few years only after the discovery of the neutron by J. Chadwick [4]. It is based on the radiological effects of radiations emitted following the in-situ neutron capture on a suitable nucleus. The target nucleus is best selected so that the capture results in energetic charged particles, which have a short range in tissues and a high specific energy loss (dE/dx) for maximal biological local damage. A high thermal neutron cross section and minimal residual activity are also important criteria in the selection of the target nucleus. The availability of ${}^{10}\text{B}$, a stable isotope of boron, following the rich medical literature developed on the toxicology of boron and a large cross section of 3840 barns of the ${}^{10}\text{B}(n,\alpha){}^7\text{Li}$ reaction for thermal neutrons have made this nuclide appropriate in the modality called Boron Neutron Capture Therapy (BNCT). On absorption of a thermal neutron by ${}^{10}\text{B}$, the excited ${}^{11}\text{B}$ nucleus promptly (~ 10 -12 s) decays to two charged particles (α and ${}^7\text{Li}$) accompanied with high probability by a 478 keV

γ -ray. The emitted charged particles α and ${}^7\text{Li}$ sharing a total energy of 2.31 MeV (1.47 MeV and 0.84 MeV, respectively) are highly-ionizing particles with short range in organic matter ($\sim 9 \mu\text{m}$ and $\sim 5 \mu\text{m}$, respectively) that are similar to the size of a single cell. The implementation of Boron Neutron Capture Therapy (BNCT) as a cancer radiotherapy requires an intense and practicable source of low energy (epithermal) neutrons. For many years, suitable neutron sources for BNCT were constrained to nuclear reactors. A reactor can produce a sufficient neutron flux (estimated to $\sim 10^9 \text{ n/cm}^2/\text{s}$ [5]) at an irradiation facility beam port for therapy duration of 30-90 min (see [6]) but suffers significant drawbacks in suitability and availability.

Worldwide efforts to design an accelerator-based neutron converter have focused on the use of lithium through the reaction ${}^7\text{Li}(p,n){}^7\text{Be}$ [7-13] at proton energies of 1.9-2.8 MeV, which produces average neutrons energies in the range 25 - 500 keV. However, a reliable conventional lithium target working under beam power levels (\sim tens kW), as considered for therapy purpose in the energy range above, proves very difficult to build because of the mechanical, chemical and thermal properties of lithium (principally its low melting point at

* Corresponding authors: Ido Silverman (ido@soreq.gov.il), Michael Paul (paul@vms.huji.ac.il)

† Deceased

181°C). The development of the liquid-lithium target LiLiT as a high-intensity epithermal neutron source, operated in conjunction with the SARAF linear accelerator has led us to investigate its application for neutron radiotherapy [1, 14, 15].

The source strength of epithermal neutron spectrum (0.1 eV - 10 keV) optimal for BNCT clinical use is considered to be of the order of 10^9 n/cm²/s, together with minimizing fluxes and dose rate of thermal neutrons (causing collateral dose to surface tissue without penetrating to a deep-seated tumor) and of fast neutrons (causing collateral dose to healthy tissue through knock-out protons). A beam-shaping assembly is therefore necessary for the tailoring of the ⁷Li(p,n) neutrons to an optimal spectrum, together with a shield for reducing the accompanying gamma dose. In order to respond to these demands, it is estimated that the proton beam power on the lithium target must be of the order of 30-50 kW for proton energy in the range 1.91-2.5 MeV.

The present project was aimed at the design and realization of a high-power liquid-lithium target compatible with the neutron fluxes required for BNCT, as far as both spectrum and intensity are concerned.

2 Thermal and mechanical design of the system

2.1. Heat transfer calculations

Heat transfer calculations of the Boron Neutron Capture Therapy (BNCT) target were performed using the commercial ANSYS-Fluent 17.2 software. The current simulations concentrated on the mitigation of the excessive evaporation risk. In order to examine the required velocity, enabling safe operation of the system, the inlet velocity and the values of the beam power were varied in the range of 1-20 m/s and 5-50 kW, and the temperatures and evaporation rates were examined for these conditions. A laminar solver was employed to solve the Navier-Stokes equations together with the energy equation for heat computations. Solving the equation with the assumption of a laminar flow is the worst case in terms of temperature analysis as turbulence enhances heat transfer in the fluid. Figure 1 presents the estimated mass evaporation rate as a function of lithium velocity and beam power. These results are for a 50 mm wide nozzle and gaussian beam parameters of $\sigma_x = 8$ mm and $\sigma_y = 12$ mm, which have been chosen from mechanical and neutronic considerations. Acceptable conditions regarding evaporation rate, up to 10 mg/h (established according to the experience with the original LiLiT system), are below the double black line. Based on these simulations, it was found that the system will be able to dissipate ~30 kW proton beam with lithium jet velocity of ~6 m/s which was achieved with the original LiLiT system. For 50 kW beam power a 13 m/s lithium jet velocity is required to maintain evaporation below ~10 mg/h. It will be available with the system upgraded design describe hereby. The lithium jet thickness was set to 1.5 mm, well above the stopping range of 2.5 MeV protons.

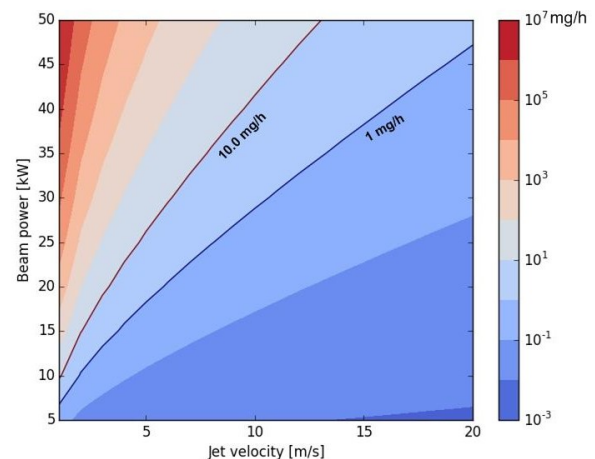


Fig. 1. Mass evaporation rate as a function of lithium velocity and beam power, for a gaussian beam parameters of $\sigma_x = 8$ mm and $\sigma_y = 12$ mm. Acceptable conditions regarding evaporation rate are below the double black line (evaporation rate below 10 mg/h). A more conservative operation limit of 1 mg/h is marked by a single black line

2.2 System final design and fabrication

The liquid-lithium nozzle, a critical component in the system, has been designed based on water experimental simulations, since water flow at 20°C and lithium flow at 225°C have almost identical Reynolds numbers. A water loop for the water simulation experiments was designed and built (Figure 2a) to create water flow velocities up to 20 m/s through the nozzle.

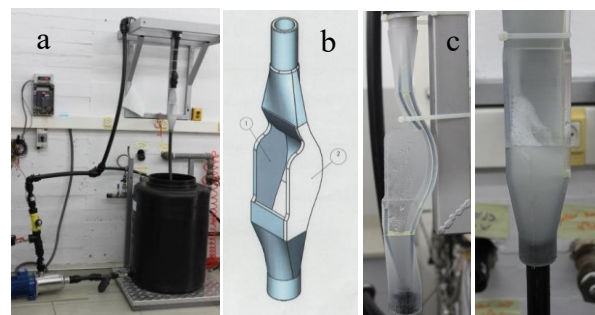


Fig. 2. a) A water loop for the nozzle design water simulation experiments; b) a preliminary wide nozzle design; c) wide nozzle during water experiments (water piles up below the nozzle at a velocity of ~10 m/s)

A preliminary wide nozzle was designed (Figure 2b) and a plastic model of the nozzle was built and tested in water flow simulation system (Figure 2c). A stable water film with a smooth surface was created when the jet velocity was below 10 m/s. At velocities above ~10 m/s (above ~0.75 l/s) water was seen piled up downstream the nozzle (Figure 2c), probably due to a bottleneck in the flow exit back to the 1" pipe. The final design has a 2" outlet pipe to provide enough through put for the low velocity return flow.

The 50 mm wide lithium nozzle optimized for high power but small source size has been designed based on

the results of these water tests. The new design (see Figure 3) features an improvement in system maintenance by providing a method to replace the nozzle without changing the whole irradiation chamber and providing a backup method of heating the nozzle with internal heaters. The new design also features a method to deal with accidental lithium spillage into the irradiation chamber which had been an operating issue with the original design.

In addition, a revised version of the lithium heat-exchanger (HX) has been completed and produced. The new HX is designed to provide higher cooling rate, better response to thermal cycles and to reduce the risks of oil leak from the cooling loop, with long helical oil tubes and minimum welded joints. It also contains two connecting ports for electromagnetic pumps (EMP), one for the original rotating magnets EMP type at the middle of the HX height and a second at the bottom to connect to the new Annular Linear INduction (ALIN) type pump being commissioned. The new design also provides a method for lithium replacement. It is presented in Figure 4.

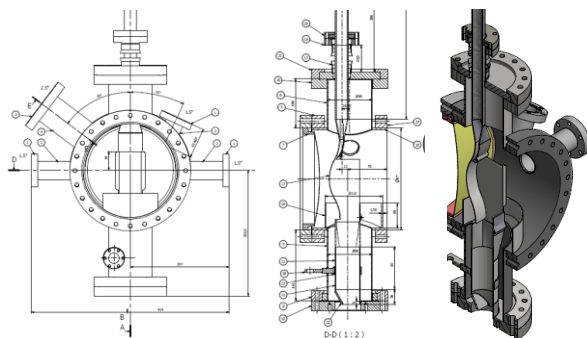


Fig. 3. The final design of the full power wide nozzle and the nozzle chamber



Fig. 4. on the left, a model of the revised full power version of the lithium heat exchanger, and at the right side a picture of the internal part before final welding

2.3 The ALIN pump design

For this project we reconsidered our choice of EMP lithium pump. The BNCT system requires a highly reliable, low-maintenance and efficient device (pump) for providing continuous circulation of liquid Li in the LiLiT system. The pump must be hermetically sealed and capable to work uninterruptedly for a long time without leaks, at high temperature and in contact with radioactive and chemically aggressive material. Mechanical pumps - centrifugal or positive displacement - were rejected as unable to satisfy the above requirements. An induction

magneto-hydrodynamics (MHD) pump was eventually selected.

Based on the thermal design, the following pumping parameters were specified for the nominal working point (at maximal pump efficiency): volumetric flow rate $Q = 2 \times 10^{-3} \text{ m}^3/\text{s}$, pumping pressure $P = 2 \text{ bar}$.

Three possible MHD pump types were considered:

1. Helical induction pump driven by fast rotating permanent magnets
2. Annular Linear Induction pump driven by 3-phase AC magnetic system (ALIN type)
3. Helical Induction pump driven by 3-phase AC magnetic system (HIP type)

Type 1 pump, having a rotating part, has been evaluated as requiring more maintenance than the induction types and hence as a possible cause of higher radiation dose exposure for the operating staff.

Reduced scale laboratory helical pump driven by AC inductor (HIP) was built and tested in the BGU MHD laboratory. The pump was designed and built for use with an existing laboratory 3-phase inductor of rotating magnetic field. The laboratory inductor could generate relatively weak magnetic field (up to 50 mT), such that the estimated pumping pressure was limited to 0.5 bar. The pump successfully produced the design pressure. However, the experiment revealed an inherent weakness of this design – high friction losses in the multi-turn helical channel.

A numerical code was developed for computation of the pump geometric, hydraulic and electric parameters. Some of the selected design parameters for the two ALIN pumps built (the prototype laboratory version and the final BNCT system version) are given in Table 1.

Table 1. Design and tested parameters of the two ALIN pumps

Parameter	Symbol	Units	Value	
			Lab. pump	BNCT pump
Total pump diameter	D_{max}	m	0.35	0.378
Total pump length	L_{max}	m	0.72	0.72
Length of active zone of the inductor	L_a	m	0.684	0.684
External diameter of the annular channel	D_c	mm	82	112
Annular channel gap	Δ	mm	3	4
Diameter of ferromagnetic core	d_{fc}	mm	67	100
Number of electric coils	N_c		18	24
Magnetic field in the channel gap	B	T	0.167	0.247
Diameter of the coil wire	D_w	mm	3	2.76
Number of wire windings in a bundle	N_w	-	70	36
Mean LM flow velocity	V	m/s	2.73	3
Synchronic velocity of magnetic field	V_s	m/s	11.4	8.4
Mean slip	$S = 1 - V/V_s$		0.76	0.64
Electric current in a phase	I	A	18	40
Magnetomotive force	MMF	A·turns	7560	11520
Total active electric power	W_E	W	3495	8350
Hydraulic efficiency of the pump	η	%	14	17

Conceptual representation of the ALIN type pump is shown on Figure 5. Linear induction pumps use a traveling magnetic field wave created by 3-phase currents. The induced azimuthal currents and the radial component of the traveling magnetic field generate a Lorentz force pushing the liquid metal along the channel annulus. The three-phase winding arrangement for the solenoids usually follows the sequence AA ZZ BB XX CC YY

where A, B, C denote the balanced three-phase winding and X, Y, Z the opposite phase.

In order to test the new pump design, a low temperature version of the pump operating with Galinstan (Ga-In-Sn, liquid metal at $>16^{\circ}\text{C}$) alloy was built and tested before the final high temperature version operating with liquid Lithium was built. Experimental circuit equipped with control valves, Venturi flow-meter, electronic pressure transmitters, three-phase transformer with variable voltage supply, programmable variable frequency power supply, frequency converter and gauss-meter for measurements of magnetic field induction was built to test the performances of this pump. The liquid metal flow-rate and pump pressure were measured at different electrical currents and frequencies. At any given set of electrical parameters, the flow rate is controlled by closing/opening control valve. The prototype pump was tested with two possible 3-phase connections – “star” and “delta”. The characteristic Pressure-Flow rate curves at 50 Hz with “star” phase connections are shown on Figure 6.

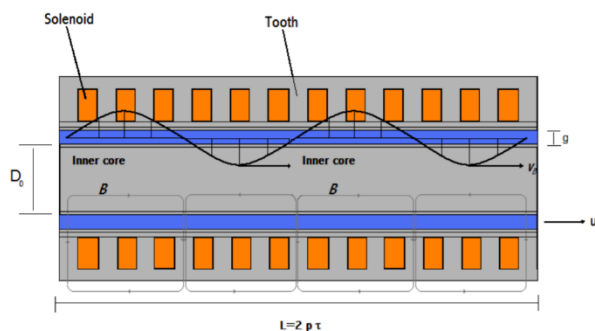


Fig. 5. Conceptual representation of the ALIN pump. The black curve schematically represents the magnetic induction (B) as a traveling wave of velocity vs. Liquid metal is shown in blue (reproduced from [16])

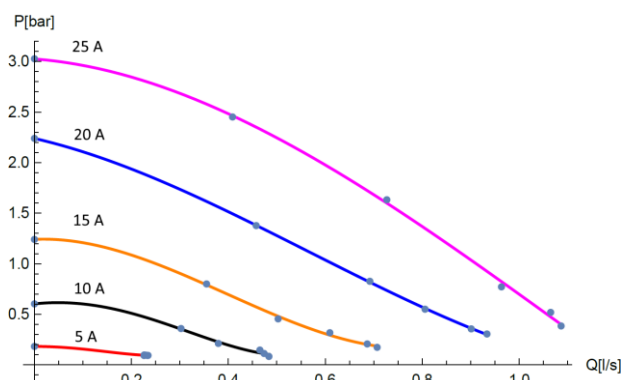


Fig. 6. The characteristic P-Q curves at different phase currents

The tests show that the pump did not achieve the required working head-flow-rate point with star connection. Delta connection was tested next. The line voltage with this connection is higher (380 V), thus the pump can operate at higher current. The maximal “shut-off” pressure of 10 bar was measured. However, the flow-rate remained below the design value. Based on these results new design parameters for the BNCT high temperature (300°C) lithium pump were specified (see right column in Table 1) and a new version has been designed and manufactured (shown in Figure 7).



Fig. 7. A picture of the high temperature (300°C) liquid Lithium ALIN pump

3 LiLiT-BNCT loop system and operation safety

The LiLiT prototype target was decided to be decommissioned in 2016 following a leak developed in the lithium reservoir, in favor of the new design. In order to support the ongoing astrophysics and nuclear research program ([1, 2]) the construction of the new design has been divided into two stages. First, a low power (6 kW) model of the new design with a narrower nozzle (18 mm wide) and a rotating-magnets EMP was built and commissioned at SARAF in 2018. The system was designed to allow relatively easy replacement of loop components (nozzle, lithium chamber and pump). The new target as installed at SARAF phase-I target room is presented in Figure 8. First irradiation test took place in December 2018 and it is used since to produce neutrons. Then, as the design of the 50 kW nozzle, heat exchanger and ALIN pump matured they were manufactured and will be integrated into the operation system at a later date.

A major concern of operating a liquid lithium target is the safety issue of protecting a few kg inventory of radio-active liquid lithium. LiLiT-BNCT contains about 7 kg (15 liter) of metallic lithium. In case of leak in the vacuum vessel of the system, air might enter the vessel or liquid lithium might flow out. In both cases a reaction of the lithium with humidity in the air or with water might release hydrogen and heat. A combination which might cause fire or explosion which will disperse radio-active ^7Be contained in the lithium. Although the risks of this scenario are rather low, a defense-in-depth concept (borrowed from the nuclear industry) has been adopted in the design. The concept asks for evaluation of the failure scenarios of a specific design and providing mitigation plans and mechanisms to protect the environment assuming any one of these failures occur. Then, the evaluation is done again for the system with the additional protection level for scenarios when even the protection layer has failed. This sequence is repeated for several cycles until the estimated probability of total failure is as low as requested.

For the LiLiT target the primary failure scenarios which are of safety concern are that the particle beam heats an un-cooled part of the target or the nozzle when there is no lithium flow. Additional scenario is a break in a liquid lithium pipe which spills liquid lithium out (a low probability event). To mitigate the first scenario, the following protection measures are used:

1. A cooled collimator with current detection is placed in front of the nozzle to identify events when the beam steers away from the nozzle.
2. A flow meter is placed on the lithium pipe and the power and running of the EMP are monitored. All signals are required to be positive in order to enable the beam to bombard the target.
3. A secondary, low-vacuum chamber is located behind the nozzle. In case the beam penetrates through the nozzle into this secondary chamber, the low vacuum causes a signal in the target vacuum sensors to generate a shutdown signal for the beam.

In case this protection layer fails and liquid lithium does spill out of the target vessel it might react with the moisture in the air or some water in the vicinity of the target. To mitigate this scenario a second protection layer was designed and contains the following sub-systems:

1. The target is placed inside a stainless steel containment vessel to limit the immediate affected zone.
2. No water or water cooled systems are placed in this containment and a dry air is supplied to have a very low humidity environment (< 5% relative humidity) which reduces the risks of lithium reaction with water or fire if a spill occurs.
3. Cameras and smoke detectors are placed in the containment to identify lithium leak if other sensor fail to identify it.

Then, if this second protection layer fails and the spilled lithium starts to react with water or moisture, a duplicate lithium fire extinguisher system using graphite power is available for manual operation from the control room. For any case, a ventilation system was installed to transfer lithium gaseous reaction products into a scrubber which will safely handle these products.



Fig. 8. Picture of the LiLiT-2 system installed at SARAF new target room with the frame of the containment vessel

This safety protection scenario was approved and a license to operate LiLiT as an intense neutron source was issued by the Israeli nuclear safety authority.

4 Neutron yield and energy spectrum

The energy of the generated neutrons in the liquid lithium target, although very close to the optimal BNCT neutron energies, should be slightly moderated. In order to provide a therapeutic neutron beam, a special moderator/reflector assembly named Beam Shaping Assembly (BSA) was designed to maximize the epithermal neutron flux Φ_{epi} while minimizing fast and thermal neutrons fluxes and shield from gamma radiation. The BSA should be installed between the neutron source and the patient.

Table 2. IAEA recommendations for a BNCT neutron source

Parameter	Symbol	Units	Value
Epithermal beam (0.5eV – 10keV)	Φ_{epi}	$\text{N cm}^{-2} \text{s}^{-1}$	$>10^9$
Fast neutron dose	$D_{\text{fn}}/\Phi_{\text{epi}}$	$\text{Gy cm}^2 / \text{Nepi}$	$< 2.0 \times 10^{-13}$
Gamma dose	$D_{\gamma}/\Phi_{\text{epi}}$	$\text{Gy cm}^2 / \text{Nepi}$	$< 2.0 \times 10^{-13}$
Thermal neutron flux ratio	$\Phi_{\text{th}} / \Phi_{\text{epi}}$		< 0.05
Directionality	J / Φ		> 0.7

As a preliminary assessment for the therapeutic effectiveness of the neutron beam, IAEA developed a set of recommended parameters for the neutron beam (ref. [5] and Table 2). Thermal neutron flux Φ_{th} (which cause radiation dose to surface tissues) must be reduced. Fast (>10 keV) neutron dose D_{fn} which accompany the incident beam, have a number of undesirable characteristics such as the production of high-LET protons, with a resulting energy dependence of their effect and must be reduced. Parasitic gamma dose D_{γ} accompanying the ${}^7\text{Li}(p,n)$ reaction must be reduced.

The beam-shaping assembly (BSA) includes mainly four parts, the moderator, the reflector, the filter for thermal neutrons and shielding for gamma radiation produced in the neutron source. The moderator has to slow down the fast neutrons yielded by the lithium target, without increasing significantly the fraction of thermal neutrons in order to get a net accumulation in the epithermal energy range (0.5 eV–10 keV). A reflector has to be included to either limit the neutron losses or scatter neutrons toward the beam port, while further improving the quality of the beam.

4.1 Simulation model

A simulation code to design a BSA that would fit the requirements for BNCT has been developed. The simulation is divided in two parts. The first of which, named SimLiT [15], calculates the neutron field produced in given conditions by LiLiT. The neutrons are then transported using the code GEANT4 [17] taking into account the geometry of the secondary target and surrounding components and materials. The SimLiT code, described in detail in Friedman et. al. [18], is a Monte Carlo program starting with a proton whose incident energy is sampled from a Gaussian distribution with given

energy mean and standard deviation (energy spread) and whose position is sampled from a given radial Gaussian distribution. It then calculates the probability of a ${}^7\text{Li}(p,n){}^7\text{Be}$ (and ${}^7\text{Li}(p,\gamma n){}^7\text{Be}^*$ to the first excited 0.411 MeV state in ${}^7\text{Be}$ when the incident energy allows it) reaction within the Li thickness until neutron threshold energy is reached, using an energy-dependent stopping power dE_p/dx taken from the code SRIM [19]. The energy-dependent differential cross sections $(d\sigma/d\Omega)(E_{p,\text{lab}},\theta_{n,\text{cm}})$ are taken from Liskien and Paulsen [20] and from Gibbons and Macklin [21] above $E_{p,\text{lab}} = 1.890$ MeV. Special care was taken for the treatment of the cross section between threshold and 1.890 MeV, where precise determination of the excitation function is crucial for correct reconstruction of the resulting neutron spectrum as discussed by Lee and Zhou [13]. The SimLiT code generates the outgoing neutron information (position vector, momentum vector and energy) which can be used as input for the following transport calculation. The SimLiT output neutron event file is used as input to a transport calculation with the code GEANT4 [22]. GEANT4 is an open source software toolkit of Monte-Carlo simulation for the passage of particles through matter. A realistic geometry and physics representation of the LiLiT and the different components of the BSA are built into the simulation. The neutron spectrum as seen at the beam port by a simulated detector is calculated. To evaluate the impact of the epithermal beam produced by the BSA in the human body a phantom head had been used, and in-phantom parameters were calculated through a set of detectors located in the phantom [22]. The phantom was designed as a simplified cylindrical phantom made from water surrounded by 0.5 mm PMMA, as reported in [22]. A full simulation of an (n,γ) reaction is impractical due to the small reaction probability; it is however highly important for a reliable simulation because of the different lengths of trajectories due to the neutron angle of emission and possible scattering inside the phantom. In order to improve the statistics for shorter calculation time we used the following method. For each neutron that enters any of the detectors, the neutron energy, $E_{n,i}$, the angle of trajectory $\theta_{n,j}$ and the length the neutron traveled inside the target, are recorded. If the energy of the simulated neutron changes inside a detector (e.g. from scattering), the new neutron energy and length are also recorded. The simulated neutron flux Φ in each detector is then calculated by:

$$\Phi_n \left(\frac{n}{\text{cm}^2 * \text{mC}} \right) = \frac{1}{AQ} \sum_j \frac{1}{\cos \theta_j}, \quad (1)$$

where A is the surface of the detector, Q is the total simulated proton charge.

Four principal physical dose components should be considered (IAEA, [5]):

1. Fast neutron dose (D_{fn}) due to the proton recoil generated from ${}^1\text{H}(n,n){}^1\text{H}$ interaction.
2. Thermal neutron dose (D_n) due to the energetic proton and the recoiling ${}^{14}\text{C}$ nucleus from the thermal neutron capture by ${}^{14}\text{N}$ via ${}^{14}\text{N}(n,p){}^{14}\text{C}$ reaction.

3. Boron dose (D_B) from thermal neutron capture ${}^{10}\text{B}(n,\alpha){}^7\text{Li}$ reaction
4. Gamma dose (D_γ) which is a combination of photon dose derived from the BSA and dose from photons induced by neutron capture reactions in tissues.

The simulated neutron fluxes were converted to the BNCT absorbed dose components along the phantom based on kerma factors for the ICRU 46 adult brain composition [22].

$$D_{En} \left(\frac{\text{Gy}}{\text{sec}} \right) = \frac{I}{VQ} \sum_j K_j * l_j, \quad (2)$$

where V is the volume of the detector, Q is the total simulated proton charge, I is the proton beam current, K_j is the kerma factor for the specific neutron energy and l_j is the length it traveled inside the detector. Boron dose rate distributions in healthy tissue and tumor tissue are calculated with different boron concentration of ~3.5 ratio between tumor and healthy tissue ($40 \mu\text{g } {}^{10}\text{B/g}$ and $11.5 \mu\text{g } {}^{10}\text{B/g}$ typical for BPA compound, respectively).

4.2 Benchmarking of simulations

The SimLiT-GEANT4 simulations have been carefully benchmarked with two different papers [23], [24]. In [23] the neutron source for the BSA is a proton beam of 2.3 MeV and 10 mA combined with a solid Lithium target. It includes a Pb reflector, a moderator built out of MgF_2 and MgO and a filter made of Bi and enriched lithiated-polyethylene with ${}^6\text{Li}$ to avoid undesirable thermal neutrons and gamma rays contamination in the beam. Their calculations were carried out using the Monte Carlo MCNP code. We build our SimLiT-GEANT4 simulations according to the configuration presented in [23] (see Figure 9). Table 3 presents the neutron beam parameters calculated in [23] and through our simulation.

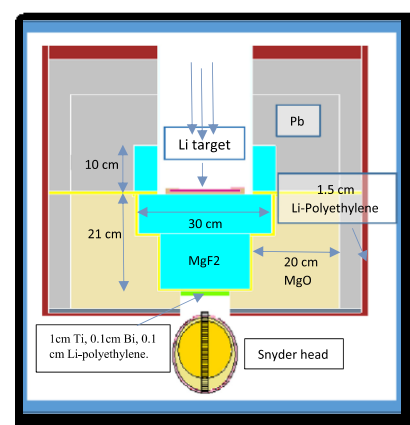


Fig. 9. The design of the BSA used in Ref. [23]

Table 3. Comparison of neutron beam quality parameters between MCNP and SimLiT-GEANT4 neutron beams designed as in [23], calculated for 2.3 MeV protons on lithium. The

discrepancy in the D_{fn}/Φ_{epi} values between the MCNP and SimLiT-Geant4 simulations is under study

Model	Φ_{epi} [10^9 n/cm ² /sec]	D_{fn}/Φ_{epi} [10^{-13} Gy cm ²]	$\Phi_{epi}/\Phi_{thermal}$	J/ Φ
MCNP	1.04	1.25	29.4	0.657
SimLiT-Geant4	1.24	4.51	21	0.607

In ref. [24], two types of neutron generation reactions have been considered. One is p-Li reaction and the other is p-Be reaction. The p-Li reaction gives larger number of neutrons than the p-Be reaction at low proton energy region around 2-3 MeV, and the neutron energy is much lower than that produced by the p-Be reaction at higher proton energy. In their work they calculated, using the Monte-Carlo MCNP code, several moderator materials including fluorine, F. From these results they decided to use the moderator materials; MgF₂ for the p-Li reaction and LiF for the p-Be reaction. We choose to benchmark the configuration of the MgF₂ 36 cm x 21 cm as moderator material for the p-Li reaction. Table 4 shows the comparison of the values required for the BNCT system.

Table 4. Calculated values for neutron epithermal flux, ratio of fast to epithermal neutrons and thermal flux for a ⁷Li(p,n) setup after moderation [24]. The Table compares values calculated with two main established transport codes (MCNP, GEANT4).

Model	Φ_{epi} [n/cm ² /sec/mA]	D_{fn}/Φ_{epi} [Gy cm ²]	$\Phi_{thermal}$
MCNP	$2.79 \cdot 10^7$	$1.0 \cdot 10^{-12}$	$3.29 \cdot 10^3$
SimLiT-Geant4	$4.51 \cdot 10^7$	$8.9 \cdot 10^{-13}$	$2.31 \cdot 10^4$

Our own design for the BSA is presented in Figure 10. In this calculation we chose to use a 2.5 MeV ± 15 keV, 20 mA proton beam that hits a 2 mm thick liquid lithium target with a beam size of 16 mm diameter. The BSA consists of 25 cm diameter Pb reflector that surrounds the target and the moderator in order to reflect back the scattered neutrons. The moderator is build out of three different materials. The first is a 20 cm diameter 20 cm long MgF₂ disk, followed by a 20 cm diameter 10 cm long Al and finally 20 cm diameter 5 cm long AlF₃. In addition a 20 cm diameter 2 cm long Pb disk is added to shield the accompanied gamma ray from the source. At the end of the BSA there is a 1 mm enriched lithiated polyethylene with ⁶Li filter to minimize the thermal neutron flux.

The phantom dimensions are 20 cm diameter and 20 cm long, with 0.5 cm polymethyl methacrylate (PMMA) walls and filled with water, simulating a targeted patient. Inside the phantom a set of 19 detectors are placed 1 cm apart in the center along the direction of the beam line. The fluxes and doses on these detectors were calculated, to give the flux/dose distribution as a function of depth in the phantom. Figure 11 shows neutron energy spectrum corresponding to the BSA at the entrance to the phantom. The energies centered at 10 keV, which is considered to be the ideal spectrum for treating deep-seated tumors. Table 5 shows current, non-optimised, calculation of the

neutron parameters, to be compared with the IAEA recommendations (Table 2).

Table 5. Calculated neutron beam quality parameters for 20 mA, 2.5 MeV proton beam in a BSA configuration as shown in Figure 11

Model	Φ_{epi} [10^9 n/cm ² /sec]	D_{fn}/Φ_{epi} [10^{-13} Gy cm ²]	$\Phi_{epi}/\Phi_{thermal}$	J/ Φ
SimLiT-Geant4	1.02	14.3	666.4	0.6

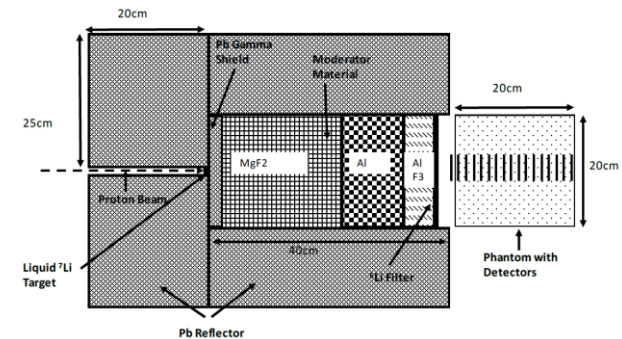


Fig. 10. BSA design for the SimLiT-Geant4 calculation

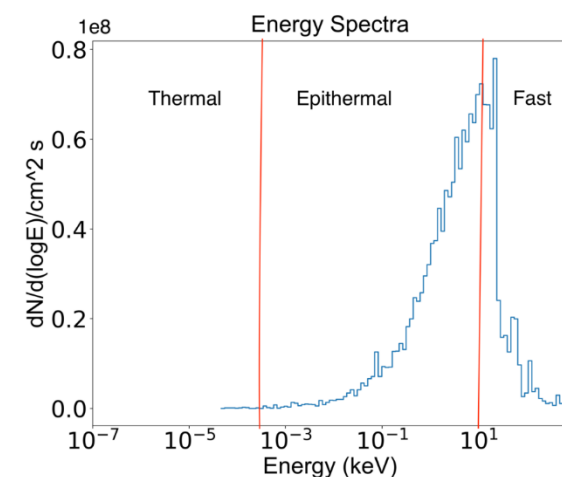


Fig. 11. Neutron spectrum at beam port of the optimized BSA

The boron dose and neutron dose distribution in the phantom were calculated according to equation (2). We rearranged them into two dose components, defined in the dose protocol prescribed for BNCT, based on clinical experience [25]. Namely, the heavy-particle dose (HCP) dose to tumor, (Boron dose to tumor + neutron dose to tumor) which should be above 15 Gy for therapeutic use and the HCP dose to healthy tissue (Boron dose to healthy tissue + neutron collateral dose to healthy tissue), which is recommended to be below 15 Gy.

The estimate of gamma-ray dose to tumor and healthy tissue is still in progress (gammas from the lithium target and gammas produced in ¹H(n,γ)²H) and is limited to 10 Gy.

Figure 12 shows the dose rate for the two components inside the phantom. The boron dose rate distributions in tumor were calculated with boron concentration of 40 μg ¹⁰B/g and the healthy tissue with concentration of 11.5 μg ¹⁰B/g.

The maximum HCP dose to healthy tissue is 15 Gy. According to Figure 12, the 15 Gy limit to healthy tissue

can be reached after 21 minutes of irradiation time. The highest dose to tumor at this time is ~ 50 Gy. The advantage depth (AD), i.e. the depth in phantom at which the total therapeutic dose in tumor equals the maximum dose of the healthy tissue, indicating the depth of effective beam penetration, is 9.4 cm.

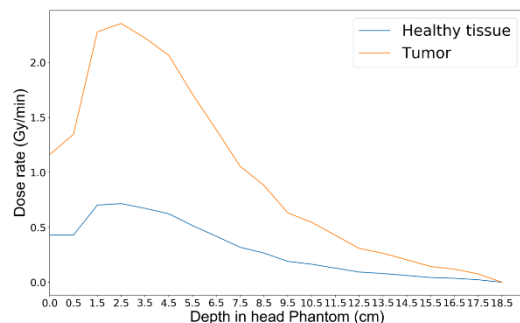


Fig. 12. Dose rate profiles in tumor and healthy tissue

5 Summary

A compact Liquid Lithium Target (LiLiT) has been operating at SARAF for several years with beam power of several kW (1.9-2.5 MeV, up to 2 mA). An upgraded model was considered to expand possible applications to Boron Neutron Capture Therapy (BNCT) and material-science studies. The improved version has been designed to sustain 50 kW beam power to provide sufficient neutron flux required for clinical BNCT application (up to 2.5 MeV, 20 mA). The new model has a 50 mm wide lithium jet and beam parameters of $\sigma_x = 8$ mm and $\sigma_y = 12$ mm to enable dissipation of the higher beam power. This design is based on CFD simulation to study the evaporation risk (achieving below 10 mg/h) and validated with water flow test with a mock-up. It also has an improved heat exchanger to remove the power to a secondary cooling loop and a new ALIN pump to provide the required lithium flow rate. Other mechanical improvements facilitate the maintenance of the system and the robustness of operation.

Radiological risks due to the ${}^7\text{Be}$ produced in the reaction are reduced by using an integrated lead shielding of the lithium reservoir. An integrated neutron moderator is being designed to adjust the neutron energy to the spectrum best suited to BNCT. A major concern of operating a liquid lithium target is the safety issue of protecting a few kg inventory of liquid lithium containing radioactive traces of ${}^7\text{Be}$. In case of leak in the vacuum vessel of the system, air might enter the vessel or liquid lithium might flow out. In both cases a reaction of the lithium with humidity in the air or with water might release hydrogen and heat. A combination which might cause fire or explosion which will disperse the radioactive ${}^7\text{Be}$ contained in the lithium. Although the risks of this scenario are rather low, a defense-in-depth concept (borrowed for the nuclear industry) has been adopted in the design.

A simulation code to design a BSA that would fit the requirements for BNCT has been developed. The

simulation is divided in two parts. The first of which, named SimLiT, calculates the neutron field produced in given conditions by LiLiT. The neutrons are then transported using the code GEANT4 taking into account the geometry of the secondary target and surrounding components and materials. This code system was used to design a beam-shaping assembly to fit around the target. The therapeutic HCP dose to the tumor is ~ 50 Gy for a limiting dose of 15 Gy to healthy tissue. The estimate of gamma-ray dose to tumor and healthy tissue is still in progress as well as full BSA optimization. The effective beam penetration depth, i.e. the depth in body at which the total therapeutic dose in tumor equals the maximum dose of the healthy tissue, is 9.4 cm.

A low power (6 kW) model of the new design with a narrower nozzle (18 mm wide) and a rotating-magnets electro-magnetic pump is operating at SARAF to support the ongoing astrophysics and nuclear research program. To take full advantage of the upgraded LiLiT model, an accelerator of appropriate energy and intensity (2.5 MeV, 20 mA, ~ 50 kW) is required.

This research was supported in part by the Ministry of Science, Technology & Space, Israel.

This paper is dedicated in memory of Dr. Alexander Arenshtam which was the chief designer of the original LiLiT and made important contributions to other projects in the SARAF facility.

References

1. M. Paul, M. Tessler, M. Friedman, S. Halfon, T. Palchan, L. Weissman, A. Arenshtam, D. Berkovits, Y. Eisen, I. Eliahu, G. Feinberg, D. Kijel, A. Kreisel, I. Mardor, G. Shimel, A. Shor, and I. Silverman, *The Eur. Phys. J. A* **55**, 44 (2019).
2. I. Mardor, O. Aviv, M. Avrigeanu, D. Berkovits, A. Dahan, T. Dickel, I. Eliyahu, M. Gai, I. Gavish-Segev, S. Halfon, M. Hass, T. Hirsh, B. Kaiser, D. Kijel, A. Kreisel, Y. Mishnayot, I. Mukul, B. Ohayon, M. Paul, A. Perry, H. Rahangdale, J. Rodnizki, G. Ron, R. Sasson-Zukran, A. Shor, I. Silverman, M. Tessler, S. Vaintraub, and L. Weissman, *The Eur. Phys. J. A* **54**, 91 (2018).
3. G. L. Locher, *Am. J. Roentgenol. Radium Therapy*, **36**, 1–13 (1936).
4. J. Chadwick, *Proceedings of the Royal Society of London. Series A, Containing Papers of a Mathematical and Physical Character*, **136**, 692–708 (1932).
5. IAEA-TECDOC-1223, *International Atomic Energy Agency*, 1223, (2001).
6. R. F. Barth, J. A. Coderre, M. G. H. Vicente, and T. E. Blue, *Clinical Cancer Research*, **11**, 3987–4002 (2005).
7. O. E. Kononov, V. N. Kononov, and N. A. Solov'ev, *Atomic Energy*, **94**, 417–420 (2003).
8. K. Tanaka, H. Yokobori, S. Endo, T. Kobayashi, G. Bengua, I. Saruyama, Y. Nakagawa, and M. Hoshi, *App. Rad. and Iso.*, **67**, 259–265 (2009).

9. A. Burlon, A. Kreiner, A. Valda, and D. Minsky, *App. Rad. and Iso.*, **61**, 811–815 (2004).
10. D. A. Allen and T. D. Beynon, *Medical Physics*, **27**, 1113–1118 (2000).
11. V. Aleynik, A. Burdakov, V. Davydenko, A. Ivanov, V. Kanygin, A. Kuznetsov, A. Makarov, I. Sorokin, and S. Taskaev, *App. Rad. and Iso.*, **69**, 1635–1638 (2011).
12. C. Willis, J. Lenz, and D. Swenson, *LINAC08*, MOP063 (2008).
13. C. L. Lee and X.-L. Zhou, *NIM B*, **152**, 1–11 (1999).
14. S. Halfon, A. Arenshtam, D. Kijel, M. Paul, D. Berkovits, I. Eliyahu, G. Feinberg, M. Friedman, N. Hazenshrung, I. Mardor, A. Nagler, G. Shimel, M. Tessler, and I. Silverman, *Rev. of Sci. Ins.*, **84**, 123507 (2013).
15. S. Halfon, A. Arenshtam, D. Kijel, M. Paul, L. Weissman, O. Aviv, D. Berkovits, O. Dudovitch, Y. Eisen, I. Eliyahu, G. Feinberg, G. Haquin, N. Hazenshrung, A. Kreisel, I. Mardor, G. Shimel, A. Shor, I. Silverman, M. Tessler, and Z. Yungrais, *Rev. of Sci. Ins.*, **85**, 056105 (2014).
16. C.O. Maidana and J.E. Nieminen, *Nuc. Eng. and Tech.*, **49**, 82–91 (2017).
17. S. Agostinelli, et. al., *NIM A*, **506**, 250–303 (2003).
18. M. Friedman, D. Cohen, M. Paul, D. Berkovits, Y. Eisen, G. Feinberg, G. Giorginis, S. Halfon, A. Krása, A. J. M. Plompen, and A. Shor, *NIM A*, **698**, 117–126 (2013).
19. J. F. Ziegler, M. D. Ziegler, and J. P. Biersack, *NIM B*, **268**, 1818–1823 (2010).
20. H. Liskien and A. Paulsen, *Atomic Data and Nuclear Data Tables*, **15**, 57–84 (1975).
21. J. H. Gibbons and R. L. Macklin, *Phys. Rev.*, **114**, 571–580 (1959).
22. J. T. Goorley, W. S. Kiger III, and R. G. Zamenhof, *Medical Physics*, **29**, 145–156 (2002).
23. L. Zaidi, M. Belgaid, S. Taskaev, and R. Khelifi, *App. Rad. and Iso.*, **139**, 316–324 (2018).
24. Y. Kiyonagi, K. Asano, A. Arakawa, S. Fukuchi, F. Hiraga, K. Kimura, H. Kobayashi, M. Kubota, H. Kumada, H. Matsumoto, A. Matsumoto, T. Sakae, K. Saitoh, T. Shibata, and M. Yoshioka, *Physics Procedia*, **26**, 223–230 (2012).
25. Y. Nakagawa, K. Pooh, T. Kobayashi, T. Kageji, S. Uyama, A. Matsumura, and H. Kumada, *J. of Neuro-Oncology*, **62**, 87–99 (2003).